Experimental study of shear strength in continuous reinforced concrete beams with and without shear reinforcement

Andrea Monserrat López, anmonlo6@upv.es

Pedro Fco. Miguel Sosa, pmiguel@cst.upv.es

José Luis Bonet Senach, jlbonet@cst.upv.es

Miguel Ángel Fernández Prada, mafernan@cst.upv.es

Universitat Politècnica de València, Camí de Vera s/n, 46022, Valencia, Spain

Abstract

Shear strength of reinforced concrete beams has been profoundly studied by many experimental campaigns conducted on simply supported beams. This situation has led to implement empirical design formulations in codes that cannot be representative of other real structures, such as continuous beams. They are characterised by the potential development of plastic hinges in areas of maximum shear and by the existence of an inflection point in the shear span, but very few experimental studies on them have been conducted. This paper analyses the results of an experimental programme involving 15 beams whose main objective was to analyse the shear strength of cantilever and continuous reinforced concrete beams according to different shear reinforcement ratios.

Nine beams of 9.00 m and six of 7.00 m with rectangular cross-sections were tested under different load and support conditions, which resulted in 30 different shear tests performed in all, two tests per beam. Three different series were considered according to the shear reinforcement ratios of 0%, 0.13%, and 0.20%. Apart from traditional instrumentation, such as strain gauges and displacement transducers, digital image correlation was employed to provide accurate displacement measurements.

The results showed that the shear strength provided by concrete (different shear-transfer actions from shear reinforcement) decreased as bending rotation increased within both the elastic and plastic ranges of rotations developed in continuous beams. Moreover, this shear strength component weakened for increasing shear reinforcement ratios. Shear slenderness was redefined for continuous beams that failed after yielding of the tensile reinforcement and redistribution of internal forces. The code formulation provided by ACI 318-19, Eurocode 2 and Model Code 2010 for shear strength were checked against these experimental results, which showed that the iterative formulation that contemplates the M-V interaction considerably improved shear strength predictions from simple formulations.

Keywords

Shear test, shear strength, reinforced concrete, continuous beams, shear reinforcement, shear slenderness, bending rotation.

Highlights

- Shear strength studied in 15 continuous reinforced concrete beams
- Shear slenderness was defined for continuous beams
- Shear strength provided by concrete reduced as bending rotation increased
- Shear strength provided by concrete was influenced by the flexural reinforcement
- Shear strength provided by concrete decreased for increasing shear reinforcement ratios

Abbreviations

A_s	area of tensile reinforcement
$A_s^{'}$	area of compression reinforcement
A_{sw}	area of shear reinforcement
a	shear span (defined as $M_{1,R}/V_{R,test} + d/2$)
c	concrete cover
d	effective depth (beam section with negative flexural moment)
E_c	modulus of elasticity of concrete
E_s	modulus of elasticity of reinforcement
f_c	compressive strength of concrete measured in cylinder
f_{ct}	tensile strength of concrete
f_u	tensile strength of reinforcement
f_y	yield strength of reinforcement
l'	span distance between two potential plastic hinges in SE (defined as $(M_{1,R} + M_{2,R})/V_{R,test} + d$)
l_i	cantilever length (i = 1, 3) or span (i = 2)
l_j	segment of the span (j = a, b, c)
l_{tot}	total beam length
z	internal lever arm
M	bending moment at a given section
$M_{1,R}$	absolute value of bending moment at failure (at d/2 from section of support A in CE and from section of support B in SE)
$M_{2,R}$	bending moment at failure (at d/2 from section of applied load P_2 in SE)
M_{flex}	bending moment when flexural reinforcement is yielded
M_u	maximum bending moment at failure
P_i	applied load (i = 1,2)
$P_{i,R}$	applied load (i = 1,2) at failure
R_A	reaction in support section A
R_B	reaction in support section B
V	shear force
V_{app}	shear force applied by loads P_1 and P_2 (not including self-weight)
V_c	shear strength provided by concrete
$V_{c,test}$	shear strength provided by concrete in tests
V_{flex}	shear force corresponding to the full flexural strength of beams
V_{Rd}	predicted shear strength by design code
$V_{R,test}$	shear strength in tests
V_s	shear strength provided by shear reinforcement
$V_{s,test}$	shear strength provided by shear reinforcement in tests
γ_c	partial safety factor for concrete material properties

δ_i beam deflection under applied load (i = 1,2)

$\varepsilon_{gauge,failure}$ stirrup strain obtained from gauges at failure

$\varepsilon_{gauge,PH}$ stirrup strain obtained from gauges at plastic hinge formation

$\varepsilon_{stirrup\ CSC,failure}$ stirrup strain obtained from DIC measurements of the CSC at failure

$\varepsilon_{stirrup\ CSC,PH}$ stirrup strain obtained from DIC measurements of the CSC at plastic hinge formation

$\varepsilon_{transducers}$ stirrup strain obtained from vertical transducers

ε_u reinforcement strain at maximum load

ε_y yield strain of reinforcement

θ angle between web compression and the axis of the member

θ_B slope at support B in the SE tests

$\theta_{B,I}$ slope at support B at the end of the first phase in the SE tests

ρ reinforcement ratio of tensile reinforcement

ρ_w reinforcement ratio of shear reinforcement

ϕ nominal diameter of a reinforcing bar

ψ rotation of beams

ψ_b bending rotation of beams

ψ_{PH} rotation of beams at plastic hinge formation (yielding of flexural reinforcement)

$\psi_{failure}$ rotation of beams at failure

1. Introduction

The shear strength of reinforced concrete beams has been extensively studied, but no general agreement on the mechanical approach that explains the failure mechanism has yet been reached. The experimental studies that have focused on obtaining a more in-depth understanding of shear behaviour have been based mostly on tests performed on simply supported beams [1–4], although real structures are usually continuous beams. Consequently, the design formulation that derives from those experimental results on simply supported beams might be inappropriate for real cases like bridges or building frames.

The moment-shear interaction (M-V), characterised by the presence of an inflection point in the shear span, is a distinctive feature of structural indeterminate structures, such as continuous beams, compared to simply supported beams. In continuous beams, potential shear failure regions (intermediate supports) are subjected to maximum shear forces and bending moment simultaneously, which differs from simply supported beams because the maximum shear is concomitant with limited bending moments. Continuous beams' shear behaviour has been investigated and several experimental programmes that simulate their conditions have been conducted [5–9]. These experimental programmes reproduce continuous beams tests by testing simply supported reinforced concrete beams with one or two cantilevers that allowed an inflection point to be generated in the shear span of beams and a bending moment at the support section by applying a load at the end of the cantilever. The results show better shear behaviour for continuous beams under distributed loads *versus* simple beams under concentrated loads, which demonstrates a positive influence of flexural action on shear strength under distributed loads. This phenomenon has also been observed in the cantilever experiments conducted by Pérez Caldentey et al. [10], where cantilevers under distributed loads (greater flexural action) failed at a higher shear force than those subjected to one concentrated load (less flexural action).

In that context, well-established mechanics-based theories that consider this M-V interaction in shear behaviour, such as the Modified Compression Field Theory (MCFT) [11, 12] or the Critical Shear Crack Theory (CSCT) [13], show that the bending moment negatively influences shear strength. Both MCFT and CSCT measure the effect of the bending moment on shear behaviour through the member's flexural deformation (flexural reinforcement strains), whose increase results in diminished shear strength. However, the effect of the bending moment on shear response has been positively considered by the approach of Tung and Tue [14]. This considers that with the same shear force,

greater flexural action would obstruct critical shear crack formation, which would lead to an increased shear resistance [7].

Some models that consider the M-V interaction constitute the basis of shear formulations in several design codes. That is, in Model Code 2010 [15] and in Canadian code CSA A23.3-14 [16] the MCFT, or its simplification SMCFT, is implemented [17], whereas the CSCT with some modifications is adopted in Swiss Code SIA 262 [18]. These code formulations, which calculate the shear strength of slender members by taking into account the flexural action concomitant with shear forces, have proven the capability of accurately predicting shear strength [13, 14, 17]. Conversely, some design codes are about empirical shear formulations that have been calibrated with the test results of simply supported beams subjected to one or two concentrated loads, such as ACI 318-19 [19] and Eurocode 2 [20]. In general, the formulas of these codes have proven to be unable to properly capture the influence of the main parameters on shear behaviour, such as the size effect or the influence of the longitudinal reinforcement ratio on shear strength [3]. In particular, empirical expressions based on concentrated loads provide conservative estimates of strength for beams subjected to uniform loads [1].

In addition, no agreement about how to consider the shear strength provided by concrete and by stirrups in design codes for reinforced concrete members with shear reinforcement has yet been reached. Model Code 2010 [15], CSA A23.3-14 [16], and ACI 318-19 [19] are based on adding a "concrete term" (shear strength provided by concrete, V_c) to a "steel term" (shear strength provided by shear reinforcement, V_s). Nevertheless, Eurocode 2 [20] only considers the "steel term", although the contribution of concrete to shear strength is indirectly taken into account with the variable-angle truss model.

Regarding the M-V interaction, although the reduction in shear strength based on the longitudinal reinforcement strain is reflected in the above-mentioned codes [15, 16, 18], it is limited by the strain at the yield point of flexural reinforcement. In statically indeterminate structures however, such as continuous beams, flexural reinforcement strains may be potentially larger than the yield point because of the plastic redistribution of internal forces after yielding of the flexural reinforcement. Actually, these structures may develop plastic rotations that enable the redistribution of bending moments before reaching their full structural strength, which allow increased shear forces after yielding of the flexural reinforcement, in contrast with the shear behaviour of statically determinate structures. **Fig. 1** depicts the different structural behaviour performed by these two structural typologies. Statically determinate structures can fail in shear before yielding of the flexural reinforcement (path A, **Fig. 1**) or afterwards with a constant shear value (path

B, **Fig. 1**). However, statically indeterminate structures can fail in shear after yielding of the flexural reinforcement with increasing shear forces as their flexural capacity is not attained until all the possible plastic hinges along the structure have been developed. Therefore, shear failure after yielding can occur while shear increases (path C, **Fig. 1**), or for a constant shear value after all the plastic hinges have been developed and the structure's flexural strength has been reached (path D, **Fig. 1**). In any case, the plastic hinges of continuous beams must resist large shear forces while developing considerable rotations, which may cause shear strength to reduce due to the flexural deformation reached in these critical plastic zones.

All these failure modes were observed in the experimental programme conducted by Monserrat-López et al. [21], who developed a tests system for cantilever and continuous reinforced concrete beams with shear reinforcement. Continuous beams failed in shear with increasing shear forces after yielding of the flexural reinforcement and redistributing internal forces. These authors showed the loss of shear strength for strains larger than the strain at the yield point and its relation with the bending rotation. This reduction in shear strength for increasing bending rotation had already been experimentally proven by Vaz Rodrigues et al. [22], who tested slab strips with no shear reinforcement fail in shear with constant shear forces after yielding of the flexural reinforcement.

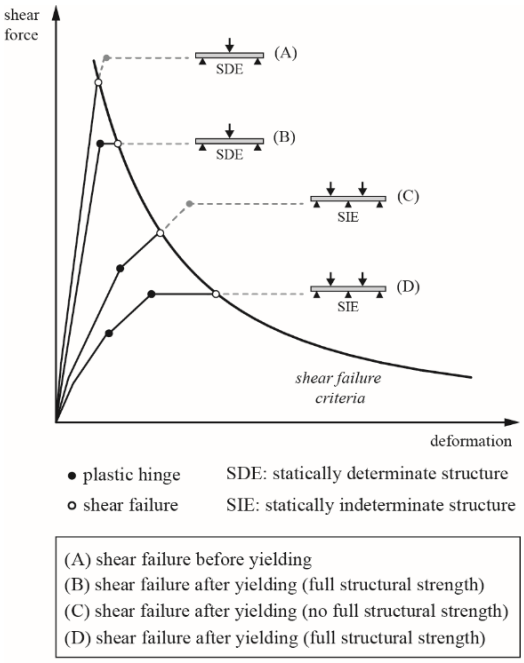

Fig. 1. Behaviour of structural determinate and indeterminate structures failing in shear before and after yielding of the flexural reinforcement.

This paper extends the previous experimental programme developed by Monserrat-López et al. [21], who studied the influence of plastic hinges rotation on shear strength in reinforced concrete statically indeterminate beams with shear reinforcement. The main

objective of this extension is to analyse the shear response of cantilever beams (statically determinate structures) and continuous beams with yielding of the flexural reinforcement and redistributing internal forces (statically indeterminate structures) according to different shear reinforcement ratios, including beams with no shear reinforcement. The two shear resistance components, that provided by concrete and that provided by steel, were studied in moment-shear interaction terms by analysing the influence of the bending rotation, which varies according to the different shear slendernesses, and longitudinal and transversal reinforcement ratios, for both statically determinate and indeterminate beams.

2. Experimental programme

2.1. Introduction

The experimental programme involves 15 beams and 30 shear tests. However, the results of the 18 shear tests performed on nine beams have already been presented [21], and the new results of the 12 tests performed on six beams are included in this paper for the first time.

In Monserrat-López et al. [21], 18 different shear tests on nine beams with shear reinforcement were presented (B1 to B9, see **Table 1**). The two shear tests carried out per beam were designed with different load and bearing points and test procedures so that each beam would fail in shear in two different ways: one as a statically determinate structure (cantilever experiment, CE) and one as a statically indeterminate structure (span experiment, SE). The main study variables were the amount of flexural tensile reinforcement and the slenderness of specimens for both the CE and SE tests. The aim was to develop shear failures with different rotation levels within a wide range of values, and both before and after plastic hinge formation.

In this paper, 12 new shear tests on six new beams are presented (B10 to B15, see **Table 1**). In this extension of the previous experimental programme, the transversal and longitudinal reinforcements were taken as the primary variables, while cantilever length and span length remained constant for the CE and SE tests, respectively. Attention was paid to the different shear behaviours of beams according to the shear reinforcement ratio (ρ_w). Different flexural tensile reinforcements were considered to allow shear failures to be developed with different degrees of bending moment redistribution. As in the previous experimental programme, two tests were run on each beam (one CE and one SE) to obtain shear failures in both statically determinate and indeterminate structures.

2.2. Specimen details

The specimens of the previous experimental programme, B1 to B9, were 9.00 m long. The new specimens B10 to B15 were 7.00 m long. They all had a rectangular cross-section (250 mm wide and 450 mm high).

Three different specimen series appeared according to the shear reinforcement ratio: (1) beams without shear reinforcement, R0; (2) beams with ρ_w = 0.13%, R1; (3) beams with ρ_w = 0.20%, R2. Shear reinforcement ϕ8/30 (ρ_w = 0.13%) is approximately (depending on each beam's materials properties) 1.5-fold the minimum amount of shear reinforcement required by Model Code 2010 [15] and Eurocode 2 [20], and twice that required by ACI 318-19 [19]. Shear reinforcement ϕ8/20 (ρ_w = 0.20%) was 1.5-fold the previously considered one. The beams without shear reinforcement (R0) and with ρ_w = 0.20% (R2) corresponded to the extension of the previous experimental programme, whereas the test results of the beams with ρ_w = 0.13% (R1) had already been presented [21]. Shear reinforcement (series R1 and R2) was arranged in the regions where shear failure was expected by two-legged closed stirrups with an 8-mm diameter and spacing of 30 cm (ϕ8/30) or 20 cm (ϕ8/20). Outside the expected failure regions, stirrups were provided in order to prevent shear failure with a reinforcement ratio of 0.90% in all specimens.

Specimens had three different sections with distinct flexural tensile reinforcement ratios to allow shear failures to develop with several degrees of bending moment redistribution. Sections had different arrangements of twelve 20 mm-diameter bars, which resulted in the three different longitudinal reinforcement ratios (ρ): (1) sections with ρ = 1.63%, S1; (2) sections with ρ = 2.29%, S2; (3) sections with ρ = 1.94%, S3 (**Fig. 2**). High reinforcement ratios were used to prevent flexural failure prior to shear failure in the SE tests. Effective depth $\boldsymbol{d}$ (distance from the extreme compression fibre to the centroid of longitudinal tensile reinforcement) was 386, 385 and 389 mm for section S1, S2, and S3, respectively.

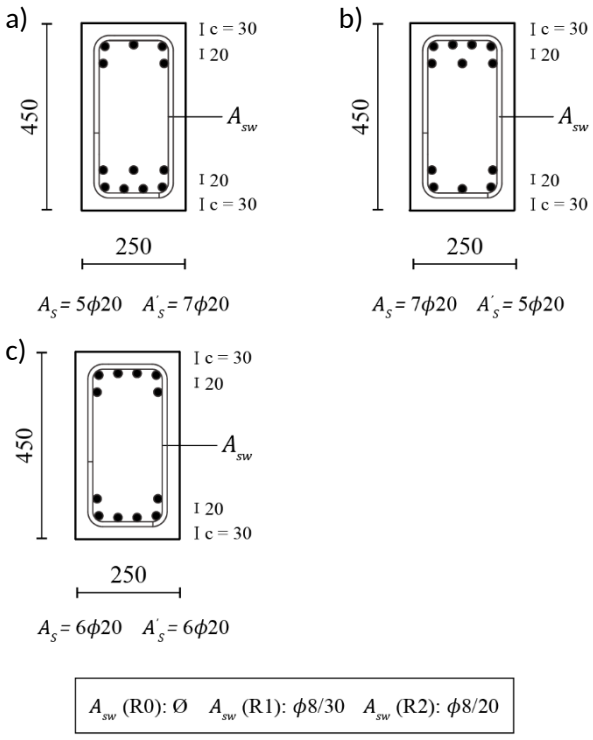

Fig. 2. Reinforcement: (a) section S1; (b) section S2; (c) section S3 (dimensions in mm).

Finally, specimens were tested with three different locations for the load and bearing points in both the CE and SE tests. This allowed to develop shear failures with different rotation levels and several degrees of redistribution of bending moments, as with longitudinal reinforcement variation.

The reinforcement and geometry of all the specimens are summarised in **Table 1**. **Fig. 3a** and **Fig. 3b** plot the detailed reinforcement and geometry of the specimens for the configuration of tests CE and SE, respectively.

A code with four terms was used to label each test conducted on specimens. The first term denoted the tested beam and the type of test (C for the CE test and S for the SE test). The second term represented the specimen series according to shear reinforcement (R0, R1, or R2). The last two terms indicated the specimen section according to flexural reinforcement (S1, S2, or S3) and the location of the load and bearing points by indicating the cantilever length (l_1) in the CE tests and the midspan length (l_2) in the SE tests (expressed after *L*, in metres). Following this notation, test B1S-R1-S1-L6 was the SE test conducted on beam B1 (B1S). The specimen had a shear reinforcement ration of 0.13% (R1), a flexural reinforcement ratio of 1.63% (S1), and a total midspan length of 6.00 m (L6).

Table 1. Reinforcement and geometry of specimens.

Spec.	Tests	A_s	A_s'	ρ (%)	ρ_w (%)	l_{tot} (m)	CE	SE				
							l_1 (m)	l_2 (m)	l_a (m)	l_b (m)	l_c (m)	l_3 (m)
B1	*B1C-R1-S1-L1 / B1S-R1-S1-L6*	5ϕ20	7ϕ20	1.63	0.13	9.00	1.00	6.00	1.00	3.10	1.90	1.00
B2	*B2C-R1-S2-L1 / B2S-R1-S2-L6*	7ϕ20	5ϕ20	2.29	0.13	9.00	1.00	6.00	1.00	2.50	2.50	1.00
B3	*B3C-R1-S3-L1 / B3S-R1-S3-L6*	6ϕ20	6ϕ20	1.94	0.13	9.00	1.00	6.00	1.00	2.80	2.20	1.00
B4	*B4C-R1-S1-L1.6 / B4S-R1-S1-L5*	5ϕ20	7ϕ20	1.63	0.13	9.00	1.62	5.00	1.00	2.10	1.90	1.00
B5	*B5C-R1-S2-L1.6 / B5S-R1-S2-L5*	7ϕ20	5ϕ20	2.29	0.13	9.00	1.62	5.00	1.00	1.50	2.50	1.00
B6	*B6C-R1-S3-L1.6 / B6S-R1-S3-L5*	6ϕ20	6ϕ20	1.94	0.13	9.00	1.62	5.00	1.00	1.80	2.20	1.00
B7	*B7C-R1-S1-L2.3 / B7S-R1-S1-L4*	5ϕ20	7ϕ20	1.63	0.13	9.00	2.31	4.00	1.00	1.10	1.90	1.00
B8	*B8C-R1-S2-L2.3 / B8S-R1-S2-L4*	7ϕ20	5ϕ20	2.29	0.13	9.00	2.31	4.00	1.00	0.50	2.50	1.00
B9	*B9C-R1-S3-L2.3 / B9S-R1-S3-L4*	6ϕ20	6ϕ20	1.94	0.13	9.00	2.31	4.00	1.00	0.80	2.20	1.00
B10	B10C-R0-S1-L1 / B10S-R0-S1-L4	5ϕ20	7ϕ20	1.63	-	7.00	1.00	4.00	0.70	1.40	1.90	1.00
B11	B11C-R0-S2-L1 / B11S-R0-S2-L4	7ϕ20	5ϕ20	2.29	-	7.00	1.00	4.00	1.00	0.61	2.50	1.00
B12	B12C-R0-S3-L1 / B12S-R0-S3-L4	6ϕ20	6ϕ20	1.94	-	7.00	1.00	4.00	0.89	0.91	2.20	1.00
B13	B13C-R2-S1-L1 / B13S-R2-S1-L4	5ϕ20	7ϕ20	1.63	0.20	7.00	1.00	4.00	1.00	1.10	1.90	1.00
B14	B14C-R2-S2-L1 / B14S-R2-S2-L4	7ϕ20	5ϕ20	2.29	0.20	7.00	1.00	4.00	1.00	0.50	2.50	1.00
B15	B15C-R2-S3-L1 / B15S-R2-S3-L4	6ϕ20	6ϕ20	1.94	0.20	7.00	1.00	4.00	1.00	0.80	2.20	1.00

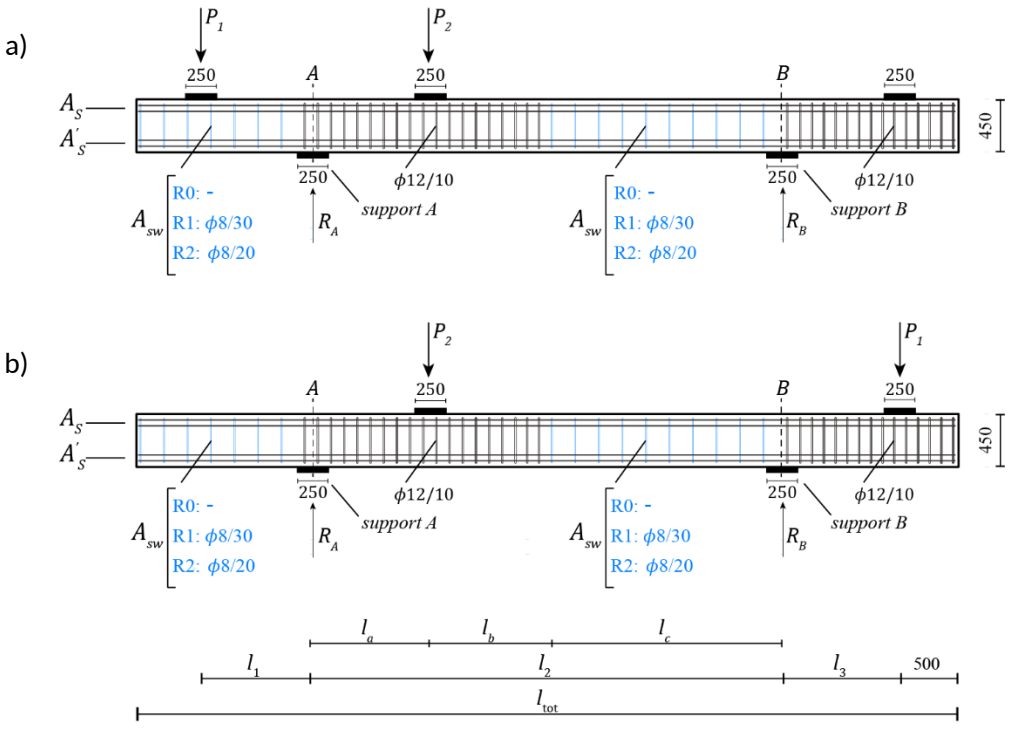

Fig. 3. Reinforcement and geometry of specimens: (a) CE tests; (b) SE tests (dimensions in mm).

2.3. Materials

The compressive strength, modulus of elasticity and tensile strength of concrete, as well as each specimen's age at the time of testing, are summarised in **Table 2**. The properties of concrete were measured according to UNE-EN 12390 [22–24] and were indicated as

the average of two tested concrete cylinders (300 mm high, 150 mm in diameter). The modulus of elasticity values corresponded to secant stiffness and tensile strength obtained from the indirect tensile strength tests. The concrete mix was 325 kg/m^3 of Portland cement, 170 l/m^3 of water (water/cement ratio of 0.52), 1065 kg/m^3 of fine aggregate (aggregate 0/4) and 825 kg/m^3 of coarse aggregate (aggregate 4/10) and concrete chemical additives (3.25 l/m^3 of plasticisers, 2.60 l/m^3 of superplasticisers). The maximum aggregate size was 10 mm.

The diameter, modulus of elasticity, steel yield stress, steel tensile strength and steel strain values at ultimate strength are summarised in **Table 3**. The reinforcement steel properties were measured according to UNE-EN ISO 6892 [26] and were the average of two tested specimens. The tension tests were load-controlled before yielding at a loading speed of 10 MPa/s, and were displacement-controlled thereafter.

Table 2. Average values of the concrete properties.

Specimen	Age at testing (days)	f_c (MPa)	E_c (GPa)	f_{ct} (MPa)
B1	33	24.1	24.3	2.5
B2	33	22.3	25.8	3.1
B3	42	22.8	24.4	2.8
B4	57	22.3	24.1	2.6
B5	71	34.7	31.2	3.6
B6	63	35.9	32.8	3.3
B7	88	36.2	34.2	2.9
B8	32	34.5	30.0	3.4
B9	39	29.7	29.4	2.2
B10	29	36.4	33.5	2.1
B11	24	31.4	31.6	2.1
B12	22	28.7	27.5	2.9
B13	31	30.6	27.3	2.5
B14	27	31.4	29.2	2.9
B15	30	26.0	26.6	2.6

Table 3. Average values of the flexural and transversal reinforcement properties.

Specimens	*B1-B3*		*B4-B9*		B10, B11 and B13		B12, B14 and B15	
ϕ (mm)	8	20	8	20	8	20	8	20
E_s (GPa)	198	218	183	213	193	226	189	206
f_y (MPa)	543	557	549	540	540	544	541	531
f_u (MPa)	677	665	651	649	642	651	662	639
ε_u (%)	9.6	10.9	11.1	13.5	10.6	21.5	10.9	18.3
f_u/f_y	1.25	1.19	1.19	1.20	1.19	1.20	1.22	1.20

2.4. Instrumentation

External instrumentation consisted of four load cells that took continuous measurements of the force in hydraulic jacks and the reaction at the bearing points. In addition, several transducers were used to measure concrete displacements, deflections and inclinations. The surface concrete displacements performed to control deformations in shear failure zones were measured with displacement transducers, with actuating rod potentiometrics of up to 150, 200, and 300 mm. The deflection at the load points was measured by the absolute non-contact position sensors integrated into hydraulic jacks and on the specimens' bottom surfaces with several displacement transducers. Two displacement transducers were used to control the inclination in the support sections. Details of the position of transducers for the specimens of series R0, R1 and R2 are found in **Fig. 4.**

Internal instrumentation consisted of strain gauges of 120 Ω resistance and a 1.5 mm measuring length. There were 31 gauges in each specimen of series R0 (**Fig. 5a**), 58 in each specimen of series R1 (**Fig. 5b**), and 40 in each one of series R2 (**Fig. 5c**).

In addition to the defined conventional instrumentation, Digital Image Correlation (DIC) was employed to perform accurate measurements of the displacement field of specimens in all the tests. More detailed information about the instrumentation of tests can be found in Monserrat-López et al. [21].

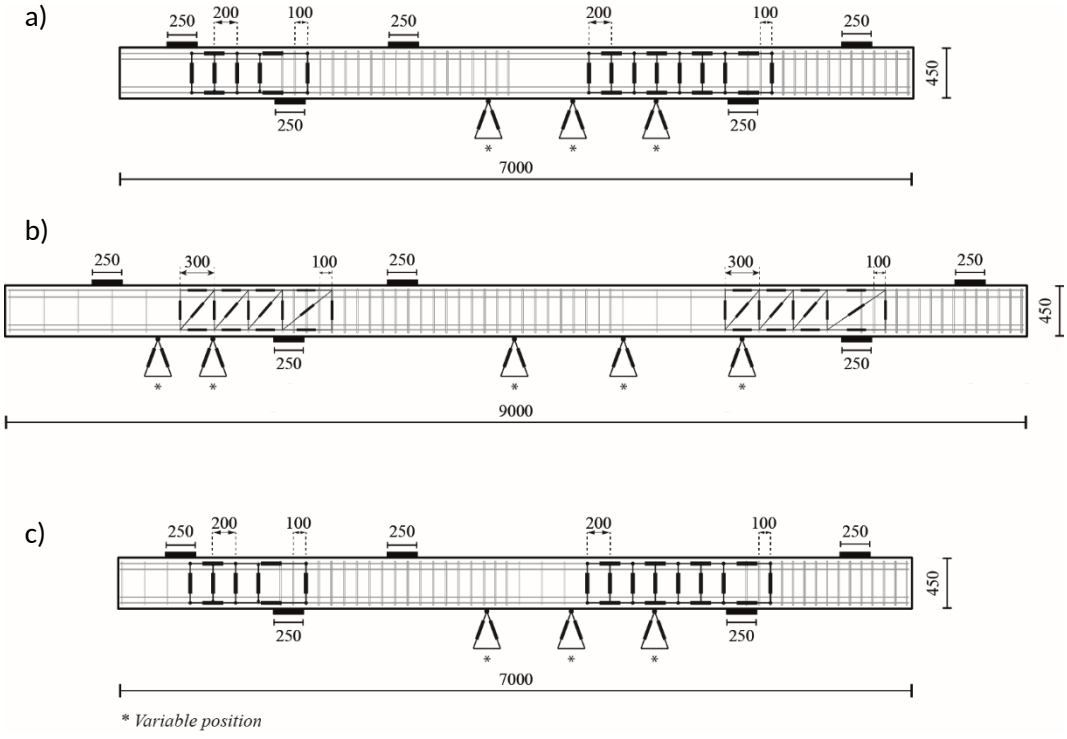

Fig. 4. Instrumentation: (a) displacement transducers of series R0; (b) displacement transducers of series R1; (c) displacement transducers of series R2 (dimensions in mm).

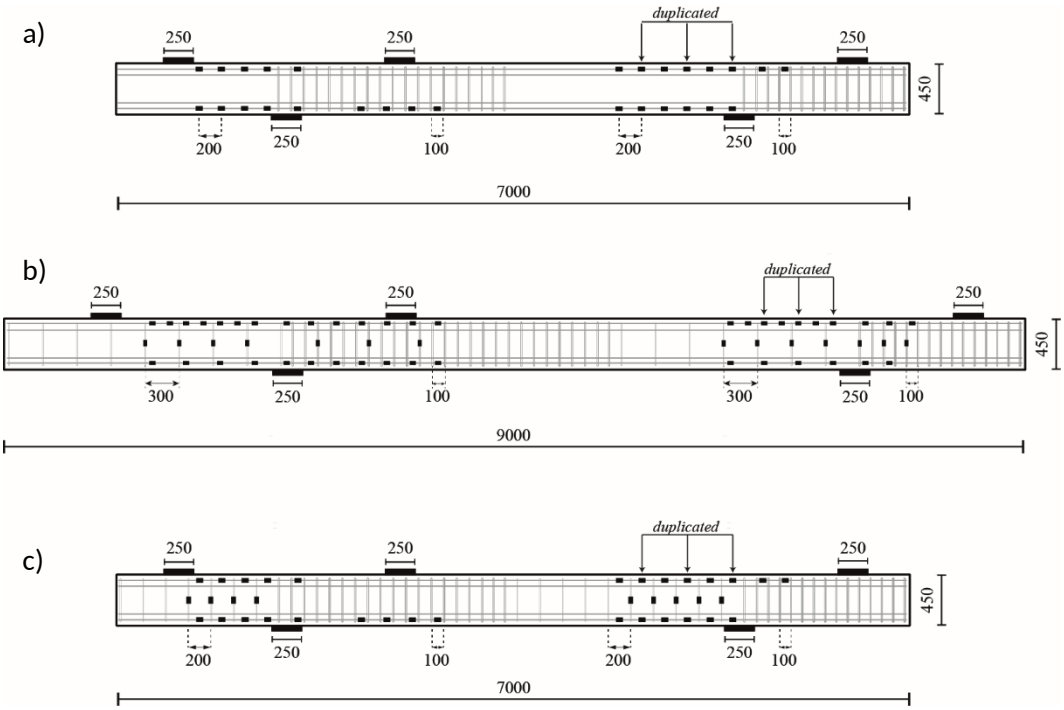

Fig. 5. Instrumentation: (a) strain gauges of series R0; (b) strain gauges of series R1; (c) strain gauges of series R2 (dimensions in mm).

2.5. Test procedure

The test setup was maintained from the previous experimental programme [21]. Loads and support reactions were transmitted to the beam through steel plates measuring 250 x 250 x 40 mm. Both bearing and load systems allowed horizontal in-plane displacements and rotations, but one of the bearing points had restrained horizontal displacement during tests.

In the CE test (**Fig. 3a**), load P_1 was applied with displacement control (0.02 mm/s) until shear failure, and P_2 was applied with load control according to the increase in load P_1 to obtain no reaction in support B. As with a statically determinate structure, shear and bending increased simultaneously with a constant shear span.

In the SE tests (**Fig. 3b**), the performed test procedure allowed shear failure to develop after yielding of the tensile reinforcement over support *B,* as well as the development of plastic rotations at the critical shear zone. Each SE test was carried out in two phases. In the first phase (**Fig. 6a**), P_1 was applied with displacement control (0.02 mm/s), and P_2 with load control, according to the increase in load P_1 to obtain no reaction in support A. This phase ended when the top longitudinal reinforcement at the support B section yielded. At this moment, the slope in that section was $\theta_{B,I}$. In the second phase (**Fig. 6b**), P_2 was applied with displacement control (0.02 mm/s), and P_1 with load control to keep the slope at the support B section blocked. In this phase, this slope was kept constant

and equal to that reached at the end of the first phase ($\theta_B = \theta_{B,I}$). This meant that, in the second phase, support B behaved as a fixed rotation support, while P_2 increased until shear failure.

It was in the second phase of the SE tests when beams became statically indeterminate structures as moments were given by compatibility conditions because of the restriction imposed for the slope at the support B section ($\theta_B = \theta_{B,I}$). In this phase, shear forces rose with increasing rotations of the plastic hinge thanks to the imposed restriction (**Fig. 6c)**. This restriction was not the equivalent to keeping the load P_1 constant in the second phase because, with an imposed P_1, the beam would simply have a continuity constant moment imposed at the support. Actually in the tested beams, slight increases in load P_1 were necessary to maintain the slope in this phase.

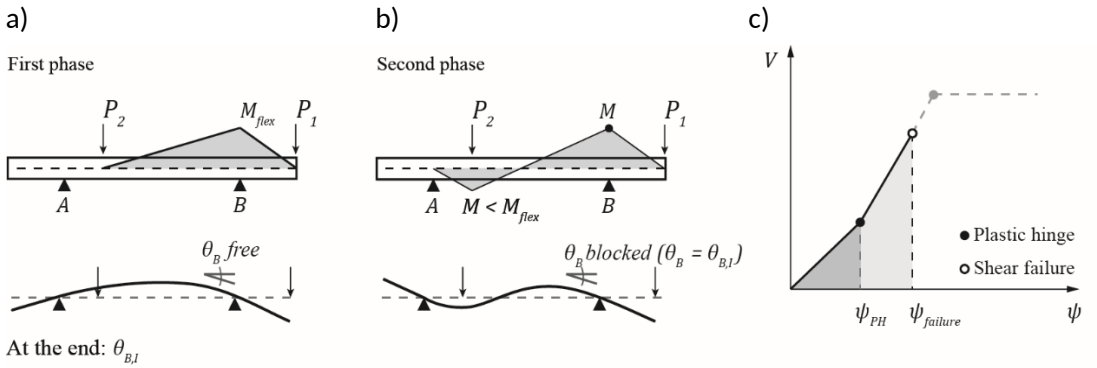

Fig. 6. Span experiment test procedure: (a) first phase of SE; (b) second phase of SE; (c) the shear forces and rotation relation in the span experiment for the two different phases.

For the specimens of series R0, it was necessary to develop a different configuration for the SE tests to avoid shear failure in the first test phase prior to the yielding of the flexural reinforcement over support B. This premature failure could occur due to the combination of both the low shear strength of beams without shear reinforcement and the high shear forces applied in the first phase of the SE tests to yield flexural reinforcement to develop one plastic hinge. The new configuration consisted in interchanging the position between support A and applied load P_2, and modifying the test procedure. In the first phase (**Fig. 7a**), P_1 was applied with displacement control (0.02 mm/s) and P_2 with load control, which was 80% of applied load P_1. In the second phase (**Fig. 7b)**, P_2 was reduced with displacement control (0.02 mm/s) and P_1 with load control according to load P_2 in so far as the slope at the support B section would remain blocked. As a result, shear failure developed during the unloading of the beam.

Specimens B10 and B12 did not develop shear failure during the unloading. Finally, they were tested by the initial test procedure (**Fig. 6**). Only specimen B11 (B11S-R0-S2-L4 test) failed in shear with the new test configuration (**Fig. 7**).

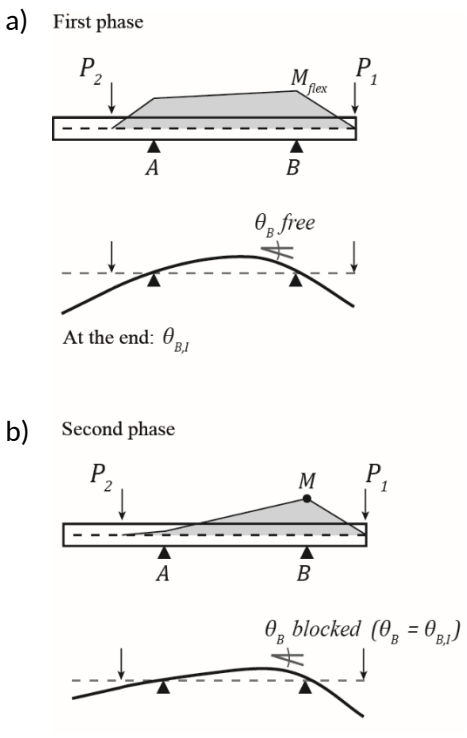

Fig. 7. Span experiment test procedure for test B11S-R0-S2-L4: (a) first phase; (b) second phase.

3. Behaviour of specimens

The behaviour of specimens in all the tests of series R0 and R2, and in the comparable tests of series R1 [21], is analysed in this section. From series R1, the considered comparable tests were those conducted on the specimens with the same loading and support conditions of the specimens of series R0 and R2. That is, the specimens with a cantilever length of 1.00 m (L1), and a span length of 4.00 (L4) for the CE tests and the SE tests, respectively.

3.1. Load deflection

In the CE tests, the load-deflection behaviour was linear until a sharp drop occurred after the maximum load (brittle shear failure) for all the tests. The stiffness of all the specimens barely changed while tests were underway. According to the different shear reinforcement ratios, the deflection under the maximum load increased from the specimens without shear reinforcement (R0) to the specimens with a higher shear reinforcement ratio (R1 and R2). The load-deflection curves (load P_1 against the

deflection under this load, $\boldsymbol{\delta_1}$) for the specimens with different shear reinforcement ratios (tests B10C-R0-S1-L1, B1C-R1-S1-L1 and B13C-R2-S1-L1) are plotted in **Fig. 8a**.

In the SE tests (**Fig. 8b**), load-deflection behaviour differed depending on the two test phases. In the first phase, the load-deflection curves had a negative slope and the applied shear reached was limited. The end of the phase was determined by the yielding of the flexural reinforcement. Thus, the first branch ended at a higher load level in the tests done with the specimens with higher tensile reinforcement (specimens with section S2) than for those with lower tensile reinforcement (specimens with section S1). In the second phase, deflection rose with an increasing applied load P_2 after the plastic hinge development in section B until brittle shear failure. Specimens showed reduced stiffness in the second phase of the SE tests compared to the CE tests performed on the same specimens. This reduction occurred because deflection was developed by the load increase after yielding of the tensile reinforcement, which meant that plastic strains developed in the plastic hinge region. The load-deflection curves (load P_2 against the deflection under this load, δ_2) for the specimens with different flexural reinforcement ratios (tests B7S-R1-S1-L4, B8S-R1-S2-L4 and B9S-R1-S3-L4) are plotted in **Fig. 8b**.

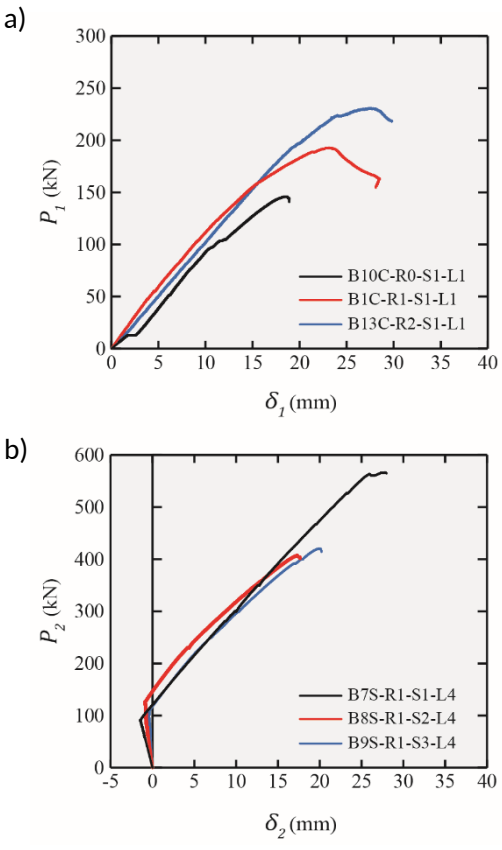

Fig. 8. Load-deflection curves: (a) CE tests according to different shear reinforcement ratios; (b) SE tests according to different flexural reinforcement ratios.

In the SE test of specimen B11 (B11S-R0-S2-L4), with a different test configuration (**Fig. 7**), load P_2 is plotted against both the deflection under the load applied at the end of the cantilever (δ_2) (**Fig. 9a**) and the applied shear (V_{app}) (**Fig. 9b**). In the first phase, both applied load P_2 and deflection considerably increased, but applied shear was substantially reduced and that avoided shear failure before yielding of the flexural reinforcement. In the second phase, despite the unloading of load P_2, which caused deflection to reduce, applied shear increased until brittle shear failure. This revealed how, despite the decrease in both the applied load and deflection under this load, applied shear increased and led to shear failure in the second test phase.

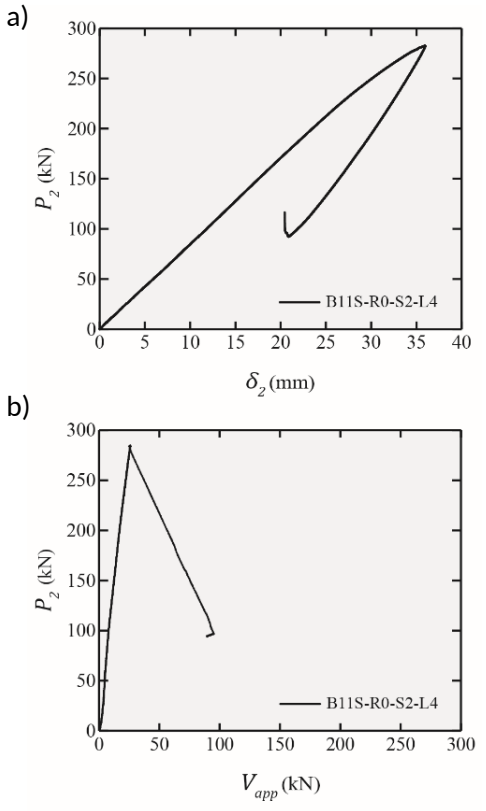

Fig. 9. (a) Load-deflection curve for test B11S-R0-S2-L4; (b) load-applied shear curve for test B11S-R0-S2-L4.

3.2. Failure mode and crack pattern

In the CE tests, shear failure developed before yielding of the flexural reinforcement (path A, **Fig. 1**) but in the SE tests, shear failure developed after yielding of the top flexural reinforcement in tension and with increasing shear force, along with the development of plastic hinge rotations (branch path C, **Fig. 1**). The crack patterns for all the tests of series R0 and R2, and the comparable tests of series R1, were analysed.

CE tests (statically determinate structures)

In all the CE tests with different shear reinforcements, specimens failed in shear before yielding of the flexural reinforcement and exhibited a similar crack pattern with an inclination of the critical shear crack (CSC, shear crack leading to shear failure) in relation to the longitudinal axis of beams, which ranged from 23 to 36 degrees (**Fig. 10**). In all the test, cracking first started as vertical flexural cracks near section A (see **Fig. 3a**). In several tests (B10C-R0-S1-L1, B1C-R1-S1-L1, B2C-R1-S2-L1, B13C-R2-S1-L1 and B14C-R2-S2-L1), as load increased, one of those flexural cracks turned towards the bearing point and developed towards the loading point to become the CSC. In the other specimens however, the CSC appeared directly from the bearing point to the loading point, and its crack width increased until shear failure. The maximum measured crack opening was approximately 3.50 mm for tests B12C-R0-S3-L1 and B1C-R1-S1-L1 (average value of the different crack widths measured with DIC along the central branch of the CSC at the maximum load), and the minimum one was approximately 1.50 mm for specimens B3C-R1-S3-L1, B14C-R2-S2-L1 and B15C-R2-S3-L1.

SE tests (statically indeterminate structures)

All the SE tests with different shear reinforcement ratios failed in shear in the second phase; that is, after yielding of the longitudinal reinforcement (plastic hinge formation) and redistributing internal forces with an increasing plastic hinge rotation. Specimens showed different crack patterns depending on the presence or absence of stirrups (**Fig. 10**). The specimens with shear reinforcement (series R1 and R2) showed a crack pattern with more uniformly distributed inclined cracks and a flatter CSC than the specimens without stirrups (series R0). For the former, the inclination of that main inclined crack in relation to the longitudinal axis of beams ranged from 20 to 35 degrees, while values ranged from 39 to 42 degrees in the latter. It is noteworthy that the specimen of test B14S-R2-S2-L4 developed a uniform crack pattern with the CSC located considerably away from the bearing plate. In the first phase, flexural cracking mainly appeared, whereas the CSC (generated from the inclination of one flexural crack) barely developed because of the reduced shear applied in this phase. In the specimens without shear reinforcement, that crack opening was in the order of 0.10 mm (average value of the different crack widths measured with DIC along the central branch of the CSC at the maximum load), but it increased to 0.50 mm in the specimens with shear reinforcement. In the second phase, the flexural cracks of the region with the plastic hinge considerably increased because of the imposed rotation. In the specimens with shear reinforcement, the CSC width increased in this phase with marked vertical movement leading to a maximum measured crack opening of approximately 2.8 mm for the specimen of test B9S-R1-S3-L4 (average value of the different crack widths measured with DIC along the

central branch of the CSC at the maximum load). In the elements without shear reinforcement, this value was 1.00 mm for the specimen of test B10S-R0-S1-L4.

In the specimens with shear reinforcement (series R1 and R2), the crack pattern determined the number of stirrups accounted for by contributing to shear strength: two stirrups for the specimens of series R1 and three in series R2. The stirrups intercepted by the horizontal branch of the CSC were not taken into account as they were considered to develop dowelling action [26, 27]. The amount of shear strength provided by stirrups (V_s) was related to the CSC width, and the more the CSC width developed at the points where it intercepted the considered stirrup, the greater the stirrup strains and, consequently, the greater its stresses. In the SE tests, the measured CSC openings increased in the second phase, especially at the end of tests, which entailed stirrups' contribution more to shear strength at that time, as confirmed by the strain measurements taken with the vertical transducers located at the position of the stirrups along the beam (**Fig. 11a** and **Fig. 11b**). To calculate the amount of shear strength provided by stirrups (V_s), employing DIC to measure the CSC width proved very useful. At the location where the CSC intercepted each considered stirrup, two points vertically aligned with it (one on each side of the crack) were considered to measure the crack opening along the vertical direction. These measurements performed by DIC allowed the strains and stresses at the reinforcement to be calculated according to the procedure established by Campana et al. [27] (explained in detail in Monserrat-López et al. [21]) and to obtain its contribution to shear strength. It is pointed out that the stirrup stains performed with gauges were not considered able to obtain their contribution to shear strength, because their location was not the exact point at which the CSC intercepted the stirrup. The measurements taken with DIC were more suitable because they gave the exact strain of the stirrup at the CSC's location. As seen in **Fig. 11c** and **Fig. 11d,** the strain measurements taken with the strain gauges located at the central point of each stirrup considerably differed from the stirrup strains calculated according to the DIC measurements of the CSC width.

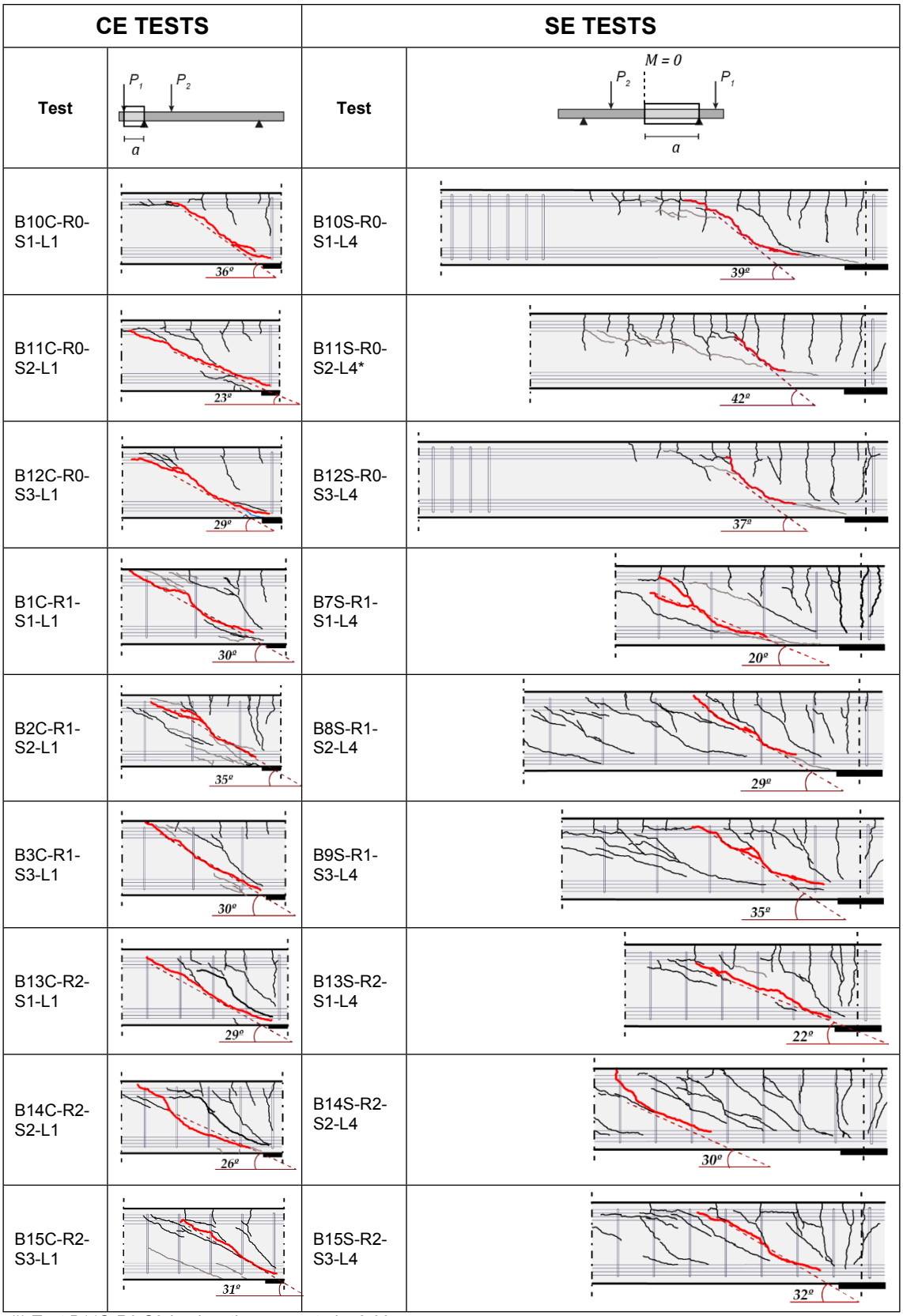

(*) Test B11S-R0-S2-L4: length represented = 2.00 m.

Fig. 10. Crack pattern for the CE and SE tests of series R0, R1 and R2.

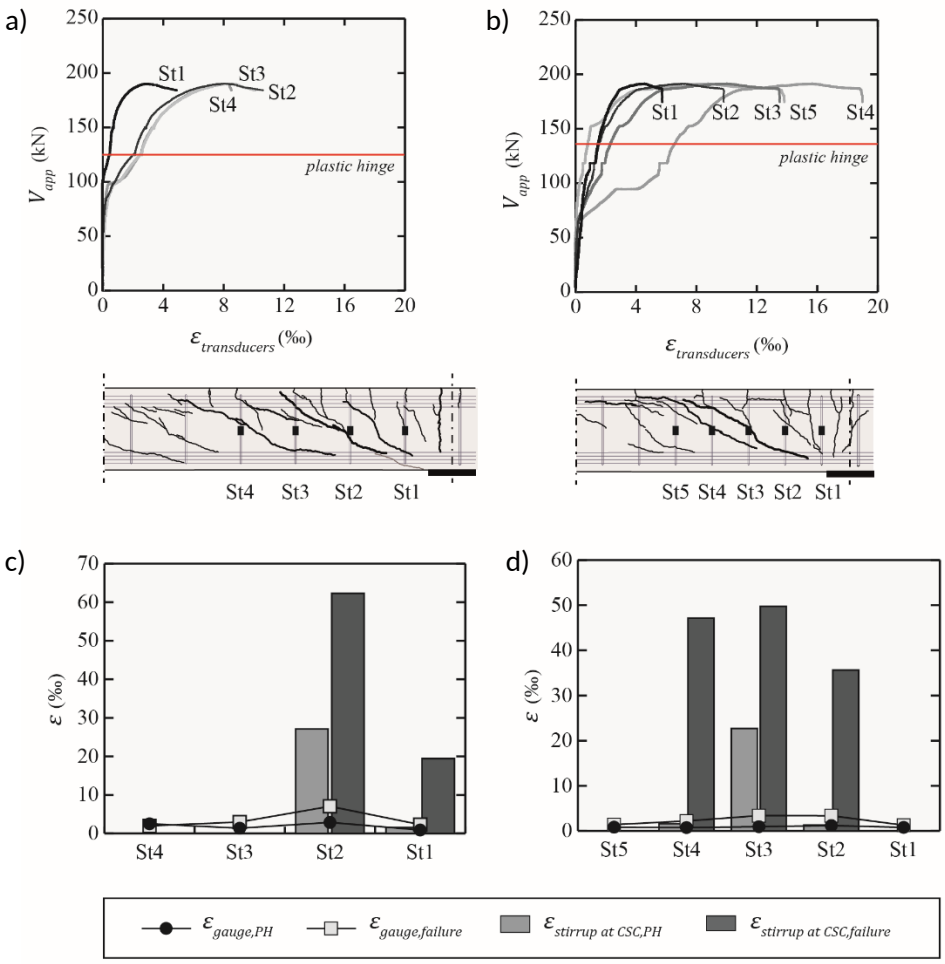

Fig. 11. Strain measurements performed with the vertical transducers located at the position of the stirrups along the beam for tests: (a) B8S-R1-S2-L4 and (b) B15S-R2-S3-L4; comparison between the strain measurements taken with the gauges located at the central point of the stirrups and strains obtained from the DIC measurements of the CSC width for tests: (c) B8S-R1-S2-L4 and (d) B15S-R2-S3-L4.

4. Discussion of the test results

The test results for the tests of series R0, R1 and R2 are discussed in this section. All the tests of series R1 are considered in this section, and their detailed results were presented in Monserrat-López et al. [21].

4.1. Shear strength

Table 4 summarises the main results of all the tests at failure, which are: the loads applied at failure ($P_{1,R}$ and $P_{2,R}$); the bending moment at failure ($M_{1,R}$) at d/2 from the corresponding support (A for CE, **Fig. 3a**, and B for SE, **Fig. 3b**); the bending moment at failure ($M_{2,R}$) at d/2 from the section of load P_2 applied for SE; the shear strength ($V_{R,test}$) provided by tests at failure at d/2 from the corresponding support (A for CE and B for SE). Shear was checked in a control section located at d/2 from the applied load [13], and the bending moment and shear force included self-weight.

Table 4. The main results at failure of the tests for both the cantilever and span experiments.

Spec.	Test	Failure mode	$P_{1,R}$ (kN)	$P_{2,R}$ (kN)	$M_{1,R}$ (mkN)	$M_{2,R}$ (mkN)	$V_{R,test}$ (kN)	$V_{s,test}$ (kN)	$V_{c,test}$ (kN)	a (m)	a/d	l'/d	ψ_b (mrad)
B1	B1C-R1-S1-L1	V (B)	192.6		157.8		196.2	123.7	72.5	1.00	2.58		10.6
B2	B2C-R1-S2-L1	V (B)	210.4		172.3		214.0	118.1	95.9	1.00	2.59		3.5
B3	B3C-R1-S3-L1	V (B)	202.1		165.2		205.8	116.7	89.1	1.00	2.56		8.9
B4	B4C-R1-S1-L1.6	V (B)	167.2		246.0		173.6	118.3	55.4	1.61	4.17		11.6
B5	B5C-R1-S2-L1.6	V (B)	208.1		304.6		214.6	119.1	95.5	1.61	4.19		13.1
B6	B6C-R1-S3-L1.6	V (B)	200.6		293.5		207.1	120.1	87.0	1.61	4.14		14.4
B7	B7C-R1-S1-L2.3	M	120.0		269.5		-	-	-	-	-		-
B8	B8C-R1-S2-L2.3	V (A)	157.8		349.5		167.1	111.4	55.7	2.28	5.93		30.7
B9	B9C-R1-S3-L2.3	V (A)	138.8		309.1		148.1	112.4	35.8	2.28	5.86		26.4
B1	B1S-R1-S1-L6	V (2 PH)	272.6	513.2	248.9	361.9	138.9	121.2	17.7	1.99	5.14	12.39	36.4
B2	B2S-R1-S2-L6	V (2 PH)	371.4	432.3	347.3	277.4	141.9	111.7	30.2	2.64	6.86	12.44	35.3
B3	B3S-R1-S3-L6	V (2 PH)	324.4	495.8	299.4	337.5	144.6	124.0	20.6	2.26	5.82	12.32	53.8
B4	B4S-R1-S1-L5	V (1 PH)	270.2	415.5	245.8	250.9	142.5	127.0	15.6	1.92	4.97	10.03	25.3
B5	B5S-R1-S2-L5	V (2 PH)	374.1	540.1	340.9	321.0	188.2	119.7	68.5	2.00	5.21	10.14	46.2
B6	B6S-R1-S3-L5	V (2 PH)	343.3	581.2	309.4	359.3	190.3	116.4	73.9	1.82	4.68	10.04	41.3
B7	B7S-R1-S1-L4	V (1 PH)	293.7	563.1	255.2	299.3	215.8	116.8	99.0	1.38	3.56	7.66	15.7
B8	B8S-R1-S2-L4	V (1 PH)	389.7	405.6	354.2	160.2	200.4	96.7	103.7	1.96	5.09	7.67	22.4
B9	B9S-R1-S3-L4	V (1 PH)	341.2	419.6	307.0	184.1	191.8	116.8	75.0	1.80	4.62	7.58	14.8
B10	B10C-R0-S1-L1	V (B)	146.0		120.2		149.7	-	149.7	1.00	2.58		8.0
B11	B11C-R0-S2-L1	V (B)	184.7		151.6		188.4	-	188.4	1.00	2.59		4.0
B12	B12C-R0-S3-L1	V (B)	116.6		96.3		120.3	-	120.3	1.00	2.56		7.9
B13	B13C-R2-S1-L1	V (B)	230.8		188.6		234.4	176.2	58.3	1.00	2.58		8.7
B14	B14C-R2-S2-L1	V (B)	263.5		215.2		267.2	171.9	95.3	1.00	2.59		8.5
B15	B15C-R2-S3-L1	V (B)	276.8		225.4		280.5	174.0	106.5	1.00	2.57		11.0
B10	B10S-R0-S1-L4	V (1 PH)	224.2	118.2	211.6	14.9	81.8	-	81.8	2.78	7.20	8.17	11.0
B11	B11S-R0-S2-L4*	V (1 PH)	363.7	94.7	349.3	-119.6	91.5	-	91.5	4.01	10.4	7.52	22.3
B12	B12S-R0-S3-L4	V (1 PH)	241.5	97.0	227.7	-1.3	87.1	-	87.1	2.81	7.23	7.69	7.6
B13	B13S-R2-S1-L4	V (1 PH)	290.6	557.2	251.8	305.9	217.0	175.3	41.7	1.35	3.51	7.66	22.0
B14	B14S-R2-S2-L4	V (1 PH)	353.5	513.8	313.9	256.8	221.9	172.0	50.0	1.61	4.17	7.68	23.9
B15	B15S-R2-S3-L4	V (1 PH)	310.5	463.4	275.0	233.9	198.6	174.5	24.0	1.58	4.06	7.59	24.6

Note: V (shear failure); M (bending failure); A (after yielding); B (before yielding); PH (plastic hinge);
*Test with different configuration: $M_{2,R}$ is the moment at $d/2$ from support A section.

The shear strength ($V_{R,test}$) obtained in the tests of the specimens with shear reinforcement was divided into its two components, that provided by shear reinforcement ($V_{s,test}$), and that provided by concrete ($V_{c,test}$), which included the different shear-transfer actions (aggregate interlock, residual tensile strength, dowelling action, and the contribution of the compression chord). The shear force provided by shear reinforcement was calculated as the sum of the tensile force of all the stirrups intercepted by the CSC (two stirrups for series R1, and three for R2). As previously mentioned, the CSC width measurements taken with DIC were employed to obtain the tensile force of stirrups

according to the procedure established by Campana et al. [27]; more detailed information about its implementation is found in Monserrat-López et al. [21]. The shear strength provided by concrete was obtained as the difference between the experimental shear strength and that corresponding to shear reinforcement ($V_{c,test} = V_{R,test} - V_{s,test}$). The $V_{s,test}$ and $V_{c,test}$ values are also presented in **Table 4**.

4.2. Shear slenderness in continuous beamsz

In **Table 4**, the equivalent shear span ($a = M_{1,R}/V_{R,test} + d/2$) and the shear span to the effective depth ratio (a/d) are provided for both the CE and SE tests. For the CE tests, shear slenderness (a/d) did not change during loading, but lowered in the second phase of the SE tests. The value provided in **Table 4** for the SE tests is the lowest, which was reached at failure.

In the CE tests, the shear strength of the specimens, represented using dimensionless parameter V/V_{flex} (where V_{flex} is the shear force corresponding to the specimen's full flexural capacity), proved to strongly depend on a/d (**Fig. 12a**). The consideration of V/V_{flex} allowed the trend of the ascending branch of the known "valley of Kani" to be obtained [29], which represents the dependency between the shear slenderness ratio and the maximum bending moment at failure in relation to the cross-section's full flexural capacity (M_u/M_{flex}).

In the CE tests, the specimens with the highest shear slenderness ratio $\boldsymbol{a/d} \approx$ 5.5 (series R1) attained their full flexural strength, as indicated in **Table 4** with "M" (bending failure) or with "V(A)" (shear failure after yielding). They failed in shear with increased deformation under constant load and extensive plastic strains in the flexural reinforcement. The specimens with the lower shear slenderness ratio, both $a/d \approx$ 2.5 (series R0, R1, and R2) and $a/d \approx$ 4.0 (series R1), failed in shear before yielding of the flexural reinforcement, as indicated in **Table 4** with "V(B)" (shear failure before yielding). The specimens with $a/d \approx$ 2.5 developed the lowest shear strength, although this strength was influenced by the transversal reinforcement ratio. For the same shear slenderness ratio, the increase in shear reinforcement allowed specimens to develop greater shear strength.

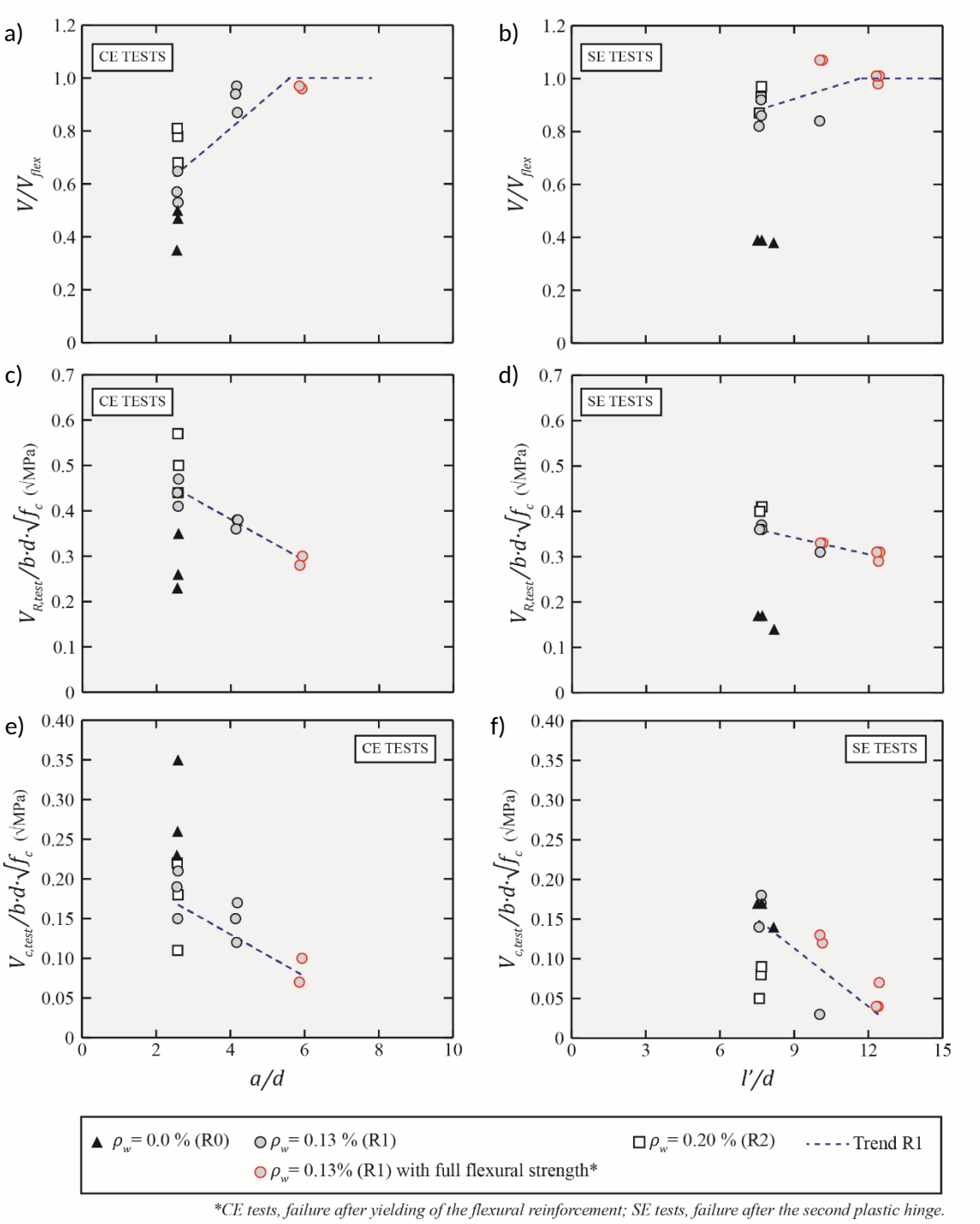

Fig. 12. Shear strength for the CE and SE tests according to the shear slenderness ratio: dimensionless parameter V/V_{flex} for (a) CE tests and (b) SE tests; total shear strength for (c) CE tests and (d) SE tests; shear strength provided by concrete for (e) CE tests and (f) SE tests. (Test B7C-S1-L2.3 not included: bending failure.)

This behaviour shows how the "valley of Kani" depends on the shear reinforcement variable [29]. The ascending branch of the valley, which limits shear failure, has a slope that depends on the shear value (V), as deduced in **Eq. 1** (flexural reinforcement considered constant), which may rise with an increasing shear reinforcement ratio. In addition, the lowest point of this branch (the minimum strength of beams), which is the

intersection with the load-carrying capacity of the arc action, shows greater shear strength for an increasing shear reinforcement ratio.

$$\frac{V}{V_{flex}} = \frac{V}{M_{flex}/a} = \frac{V\,a}{A_s\,f_y\,z} = \frac{V}{k\,A_s\,f_y}\cdot\frac{a}{d} = K(\rho_w)\cdot a/d \qquad (1)$$

It must be pointed out that in the SE tests, the shear force that corresponded to the full flexural capacity of the specimen (V_{flex}) differed from that obtained in the CE tests. The structure's full flexural capacity was not achieved when the flexural reinforcement at section B yielded. The simulated continuous beams only developed that capacity after yielding of the flexural reinforcement at section B and under the applied load P_2 (path D, **Fig. 1**). This occurred in the tests denoted in **Table 4** with "V (2PH)" (shear failure with two plastic hinges). However, the specimens that failed before full flexural capacity was reached (path C, **Fig. 1**) are denoted in **Table 4** with "V (1PH)" (shear failure with one plastic hinge).

It thus follows from developing dimensionless parameter V/V_{flex} in **Eq. 2** (flexural reinforcement considered constant) that the shear slenderness ratio (a/d), considered in the CE tests (**Eq. 1**), became factor l'/d in the SE tests. Length l' was defined as the distance between the two sections where plastic hinges, and was a suitable variable to explain the shear strength related to the full flexural capacity in a continuous beam with a shear failure after redistributing bending moments. In **Table 4**, the equivalent ratio l'/d is given for the SE tests by considering $l' = (M_{1,R} + M_{2,R})/V_{R,test} + d$.

$$\frac{V}{V_{flex}} = \frac{V}{(M_{flex,1} + M_{flex,2})/l'} = \frac{V\,l'}{A_{s,1}\,f_y\,z_1 + A_{s,2}\,f_y\,z_2} = \frac{V}{(k'_1 A_{s,1} + k'_2 A_{s,2})\,f_y}\cdot\frac{l'}{d} = K'(\rho_w)\cdot l'/d \qquad (2)$$

In **Fig. 12b,** the specimens' shear strengths from the SE tests are plotted according to factor l'/d, and a comparable correlation to that described in the "valley of Kani" [29] was obtained. As in the CE tests, dependency appeared between the shear strength according to l'/d, and the shear reinforcement ratio. With the same l'/d value, the specimens with no shear reinforcement developed much less shear strength than those with shear reinforcement.

After yielding of the reinforcement at section B and redistributing bending moments (second phase), a/d lowered with an almost constant value of $M_{1,R}$ in the SE tests. Therefore, the decrease in a/d did not mean the reduction in the bending moment in the critical zone failed in shear, that is, it did not mean the reduction in the M-V interaction, as it did in the CE tests. Therefore, whereas the interaction was properly represented

with the constant ratio a/d in the CE tests, this ratio was not suitable for the SE tests, and the l'/d ratio was used instead.

In fact it has already been pointed out that shear slenderness a/d, defined according to the location of the point of contraflexure, is not the most suitable parameter to describe the shear strength behaviour of continuous beams according to tests conducted in simulated continuous beams with redistributed internal forces after yielding of the flexural reinforcement. In continuous beams without stirrups, as tested by Adam et al. [9], no completely proportional correlation appeared between the reduction in shear slenderness (defined according to the distance between the support and the inflection point) and the increase in shear load capacity. For the continuous beams tested under distributed loads by Cavagnis et al. [8], it was stated that the point of contraflexure had no notable influence on shear strength.

For the tested specimens, the negative effect of the bending moment on shear response (M-V interaction) was obtained for both the total shear strength (the CE tests in **Fig. 12c** and the SE tests in **Fig. 12d**) and the shear strength provided by concrete (the CE tests in **Fig. 12e** and the SE tests in **Fig. 12f**). It was confirmed that, whereas the total shear strength was greater for the specimens with shear reinforcement, the shear strength provided by concrete was greater for those specimens without shear reinforcement.

4.3. Rotation

The M-V interaction was analysed in tests by the bending rotation developed by specimens at shear failure. **Table 4** shows the bending rotation values (ψ_b) at failure for all the tests. This rotation was obtained from integrating the bending curvatures (calculated from the longitudinal strains of the top and bottom fibres of the beam measured by DIC) along the length of the beams where the CSC developed. This length extended to approximately $2d$ from the support section (A for CE, **Fig. 3a**, and B for SE, **Fig. 3b**) for all the specimens, and covered the development region of the plastic hinge in the SE tests.

Fig. 13 for the specimens with ρ_w = 0.13% (series R1) depicts the increase in the bending rotation developed at shear failure with increasing shear slenderness in both the CE tests (**Fig. 13a**) and SE tests (**Fig. 13b**). This correlation between ψ_b and the slenderness of the members has already been experimentally confirmed by Vaz Rodrigues et al. [22] for members without shear reinforcement. In that experimental programme [22], the negative effect of the bending rotation on shear strength was also proven for members without shear reinforcement, and a failure criterion based on the CSCT [13] that considers shear strength reduction for increasing bending rotation for beams without

shear reinforcement developing plastic strains was proposed. For the specimens with shear reinforcement, the same reduction in shear strength provided by concrete has been experimentally confirmed by Monserrat-López et al. [21]. That is, the reduction in shear strength in the specimens with shear reinforcement for increasing bending rotations is a consequence of the reduction in shear strength provided by concrete.

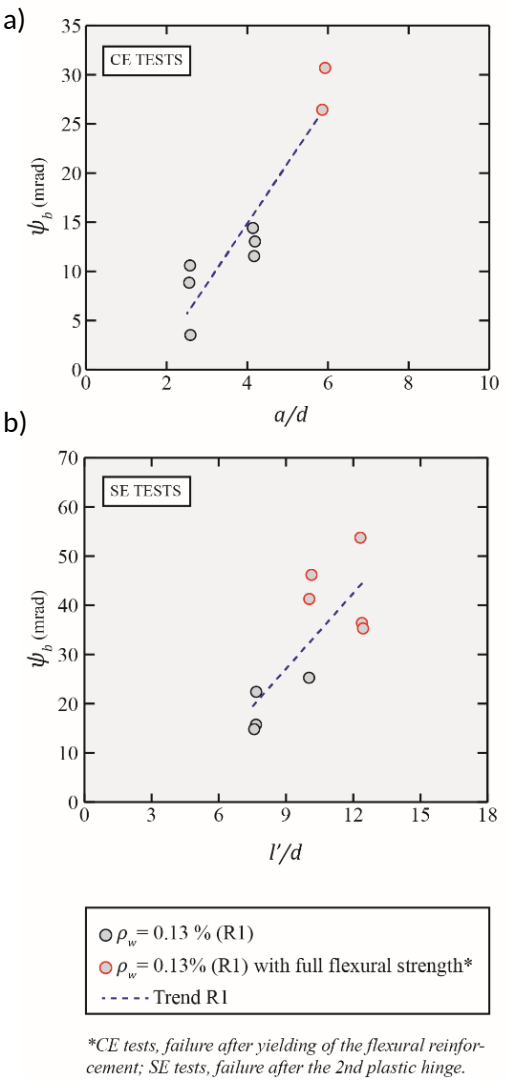

Fig. 13. Bending rotation according to the shear slenderness ratio for the tests of series R1: (a) CE tests; (b) SE tests. (Test B7C-S1-L2.3 not included: bending failure.)

The dependence between the shear strength provided by concrete and the bending rotation according to the longitudinal reinforcement ratio for the specimens with ρ_w = 0.13% (series R1) is plotted in **Fig. 14a**. This dependence enabled different levels of rotation to be reached in tested beams according to the various tensile longitudinal reinforcements, and proved that the higher the flexural reinforcement ratios, the greater the shear strength provided by concrete for the same rotation level. This can be explained by dowelling action as it grows with the amount of longitudinal reinforcement by providing

larger shear strength, particularly the shear strength provided by concrete because it is a shear-transfer mechanism through concrete. Not only did the shear strength provided by concrete increase with the amount of longitudinal reinforcement, but this increase was more significant for the larger rotations in the tested beams. Seen in **Fig. 14b**, where the value of the shear strength provided by concrete obtained from the test results trends (**Fig. 14a**) is represented *versus* the different flexural reinforcement ratios for several rotation levels, the increase in strength with the longitudinal reinforcement ratio was more pronounced for higher rotation values. That is, dowelling action was activated considerably by bending rotation. This meant that for low rotation levels, the shear strength provided by concrete was similar independently of the amount of longitudinal reinforcement. However for increasing rotations, differences in shear strength appeared according to the amount of longitudinal reinforcement.

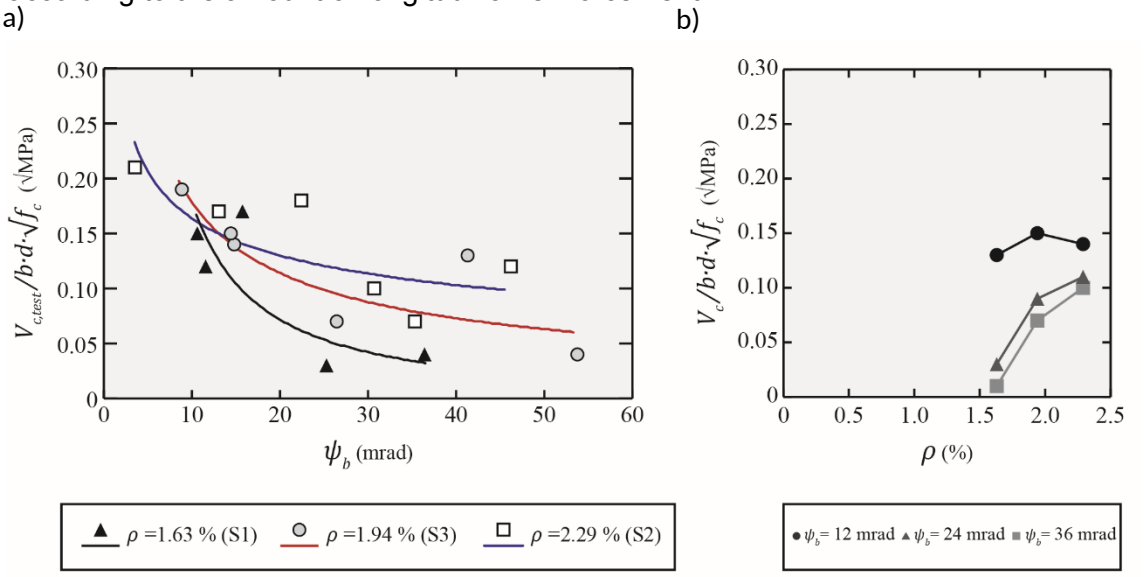

Fig. 14. (a) Shear strength provided by concrete according to the bending rotation for the tests of series R1 (Test B7C-S1-L2.3 not included: bending failure.); (b) shear strength provided by concrete obtained from the test results trends according to the flexural reinforcement ratio for different rotation levels.

Finally, it is noteworthy that the described reduction in shear strength with increasing rotation was also influenced by the shear reinforcement ratio, as observed in **Fig. 15.** Consequently, the expression proposed in Vaz Rodrigues et al. [22] should be related to the shear reinforcement provided in the specimens with stirrups.

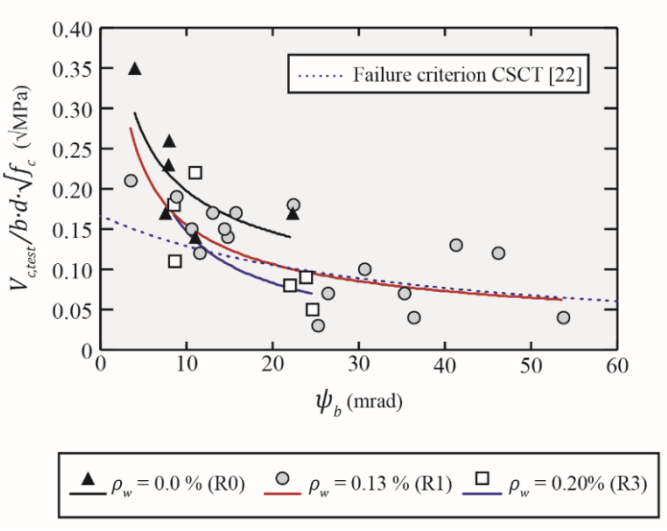

Fig. 15. Shear strength provided by concrete according to the bending rotation for the tests of series R0, R1 and R2. (Test B7C-S1-L2.3 not included: bending failure.)

4.4. The shear reinforcement ratio

The shear strength of tests CE and SE according to the different shear reinforcement ratios (series R0, R1 and R2) for the comparable tests, L1 and L4 respectively, was studied. Although shear strength noticeably improved with increased shear reinforcement (**Fig. 16a**), the shear strength provided by concrete decreased as the transverse reinforcement ratio rose (**Fig. 16b**). This meant that the shear-transfer mechanisms developed by concrete reduced for increasing shear reinforcement ratios.

In addition, the CE tests showed greater shear strength than in the SE tests for both the total shear strength and shear strength provided by concrete, but also greater scatter for all the shear reinforcement ratios (**Fig. 16a** and **Fig. 16b**). The reduced dispersion of the SE test results, compared to the CE test results, can be explained by the limited contribution of dowelling action when flexural reinforcement yields [8]. Dowelling action is a shear transfer action activated with transversal displacements of longitudinal reinforcement, so its contribution increases for higher reinforcement ratios. In the tested specimens, the high ratio of flexural tensile reinforcement may cause a considerable contribution of dowelling action to shear strength, with evident differences according to different specimen sections (S1, S2 or S3), which would cause scatter in the CE tests. However in the SE tests, with shear failures after yielding of the flexural reinforcement, the contribution of this action would reduce and, consequently, the scatter caused by it in the shear strength test results would also reduce.

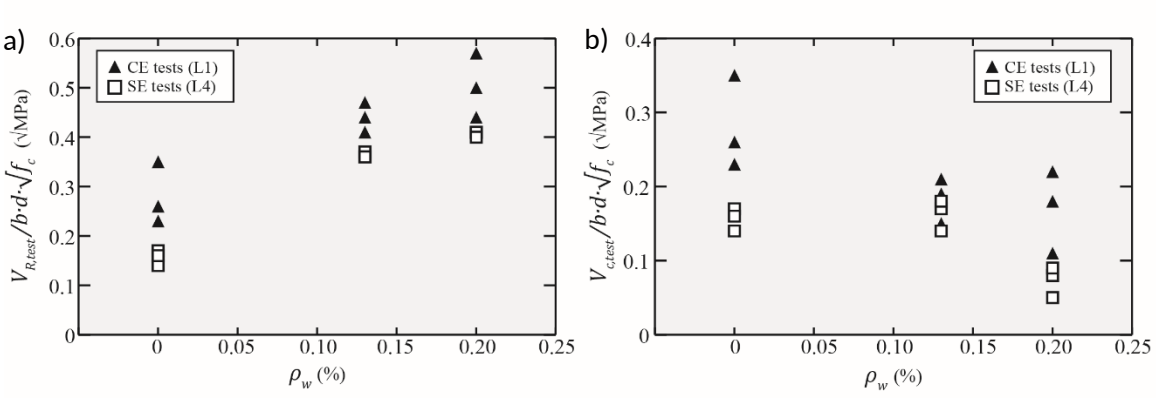

Fig. 16. Shear strength for the CE and SE tests according to the shear reinforcement ratio: (a) total shear strength; (b) shear strength provided by concrete.

5. Comparison of the test results with existing code provisions

In **Fig. 17**, the experimental-to-predicted shear strength ($V_{R,test}$ / V_{Rd}) ratio is represented according to the bending rotation at failure for all the tests (series R0, R1 and R2). For the code provisions analysis, only the CE tests with the failure mode indicated in **Table 4** by "V(B)" (shear failure before yielding) and the SE tests with "V (1PH)" (shear failure with one plastic hinge) are included; that is, 12 CE tests (specimens B1 to B6 and B10 to B15) and 10 SE tests (specimens B4 and B7 to B15).

The considered codes are ACI Building Code 318-19 [19] (**Fig. 17a**), Eurocode 2 [20] (**Fig. 17b**), Model Code 2010 (Level I Approximation) [15] (**Fig. 17c**), and Model Code 2010 (Level III Approximation) [15] (**Fig. 17d**). In all cases, γ_c = 1.0 and shear strength were optimised by considering the minimum possible angle between web compression and the axis of the member (θ).

Table 5 includes the statistics (average and COV) of the $V_{R,test}$ / V_{Rd} ratio, detailed for the different series and codes. The statistical analysis was divided into tests both without and with shear reinforcement. Accordingly, the scatter of the experimented-to-predicted shear strength ratio is always greater for those tests conducted on specimens without shear reinforcement (series R0) than for those with shear reinforcement (series R1 and R2) for all the code predictions.

The shear strength provisions predicted by codes with simple formulations (ACI 318-19, Eurocode 2, MC2010 Level I) generally show similar scatter results (**Table 5**). However, the shear strength values predicted by MC2010 Level I are very conservative for specimens without and with shear reinforcement. These "too safe" predictions may result from non-optimised angle θ, which is a fixed constant in the formulation of Level I. Despite the scatter and average results in ACI 318-19 and Eurocode 2 being similar,

they are based on very different formulations. For the specimens with shear reinforcement, the former considers the sum of the shear strength provided by stirrups according to a fixed-angle truss model and the shear strength provided by concrete obtained from an empirical calibrated expression. However, the latter considers the shear strength provided by stirrups according to a variable-angle truss model, which indirectly takes into account concrete's contribution.

The predictions provided by simple formulations can be improved with the iterative formulation based on MCFT [11, 12] from MC2010 Level III (Level II for series R0) (**Table 5**). It provides less conservative predictions and reduces scatter in the results. The formulation of this level considers the M-V interaction in shear strength by reducing shear strength according to the longitudinal reinforcement strain, which is related directly to the bending rotation. It is noteworthy that all the shear strength predictions from MC2010 Level III (Level II for series R0) were safe.

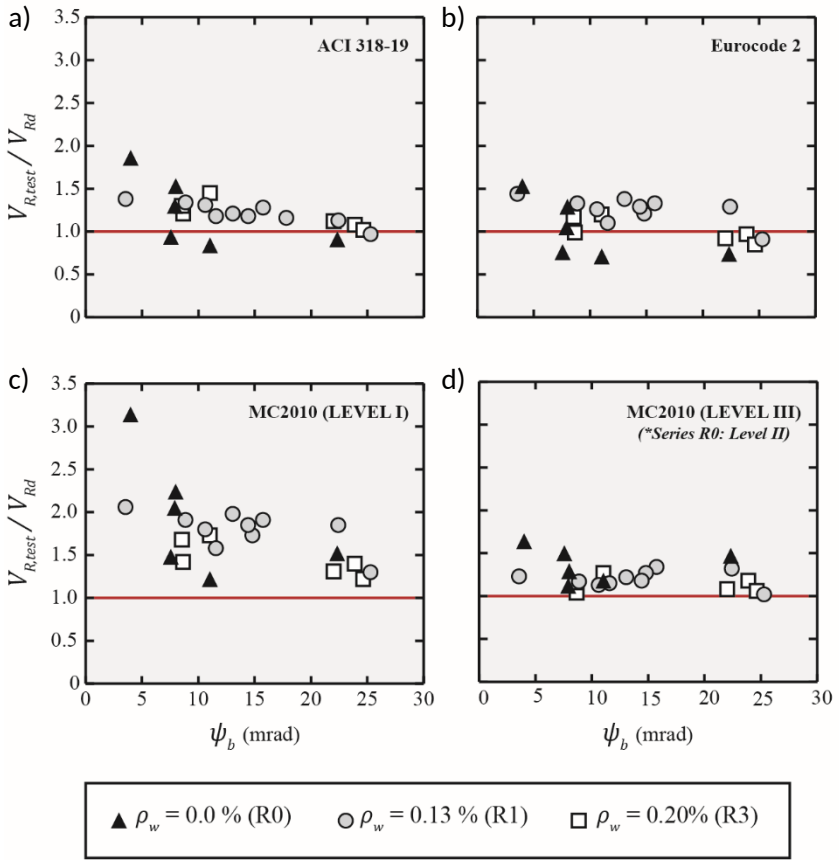

Fig. 17. Comparison made between the test results and the predicted shear strengths calculated according to design codes: (a) ACI Building Code 318-19; (b) Eurocode 2; (c) Model Code 2010 Level I; (d) Model Code 2010 Level III.

Table 5. Summary of all the test results compared to code provisions.

Analysis	ρ_w (series) [n. tests]		$V_{R,test} / V_{Rd}$			
			ACI 318-19 [19]	**Eurocode 2** [20]	**MC2010 (Level I)** [15]	**MC2010 (Level III)** *(*Series R0: Level II)* [15]
Without shear reinforcement	- (R0) [6 tests]	Average	1.23	1.01	1.94	1.37
		COV	0.33	0.33	0.36	0.15
With shear reinforcement	0.13% (R1) [10 tests]	Average	1.22	1.25	1.80	1.20
		COV	0.10	0.12	0.12	0.08
	0.20% (R2) [6 tests]	Average	1.20	1.02	1.46	1.13
		COV	0.13	0.14	0.14	0.08
	(R1 & R2) [16 tests]	Average	1.21	1.17	1.67	1.18
		COV	0.11	0.16	0.16	0.08

6. Conclusions

This paper presents the results of 12 new shear tests on six reinforced concrete beams with and without shear reinforcement. These tests complement the 18 shear tests carried out on reinforced concrete beams with shear reinforcement from the previous experimental programme [21]. The tests system used in these experimental campaigns allowed two shear tests to be conducted on the same reinforced concrete beam, one on a cantilever beam and one on a continuous beam, where shear failure occurred with growing shear forces after yielding of the flexural reinforcement and the plastic redistribution of flexural forces. The shear strength of statically determinate and indeterminate structures, with different transversal reinforcement ratios, were studied. The main conclusions drawn from these results are listed below:

1. For the beams with shear reinforcement, crack pattern (cracking shape and position) determines the contribution of stirrups to shear strength as the critical shear crack openings at stirrup sections vary the stresses developed for transversal reinforcement. Digital Image Correlation is an adequate tool for performing those crack measurements.
2. For the tested cantilever and continuous beams, the analysis of the shear slenderness ratio shows that bending moment negatively affects the shear response. However, the shear slenderness ratio for the continuous beams, which fail after yielding of the flexural reinforcement and redistributing internal forces, must be redefined by considering the distance between the two sections where plastic hinges develop to attain full flexural capacity.

3. For the beams with the same shear reinforcement ratio, the shear strength provided by concrete decreases as bending rotation increases, which can be related directly to the moment-shear interaction until tensile reinforcement is yielded. However, the tests conducted on the continuous beams show that after yielding, shear strength continues to weaken with higher bending rotation levels.
4. Loss of shear strength provided by concrete with increasing rotation is influenced by the flexural and shear reinforcement ratios. The influence of the flexural reinforcement ratio is stronger for increasing bending rotation values.
5. The contribution of concrete and transversal reinforcement to shear strength varies according to the shear reinforcement ratio of beams. Although shear strength improves for increasing shear reinforcement ratios, concrete contribution decreases with them. For higher shear reinforcement ratios, the shear-transfer mechanisms associated with concrete weaken.
6. The simple formulations from ACI 318-19, Eurocode 2 and MC2010 Level I provide similar scatter results for the experimented-to-predicted shear strength ratio, although MC2010 Level predicts very conservative values. The iterative formulation from MC2010 Level III, based on the MCFT, considers the M-V interaction and gives less conservative and scatter results.

Acknowledgements

This research was funded by grants from the Spanish Ministry of Economy and Competitiveness to Research Project BIA2015-64672-C4-4-R. The experimental programme was developed in the Laboratory of Concrete at the Institute of Concrete Science and Technology (ICITECH) of the Universitat Politècnica de València (UPV), with concrete supplied by Caplansa. Andrea Monserrat was supported by the Conselleria d'Educació, Investigació, Cultura i Esport of the Generalitat Valenciana (Order 6/2015, DOCV no. 7615 15.09.2015) with European Regional Development Funds (ERDF) allocated by the EU.

References

[1] M. D. Brown, O. Bayrak, and J. O. Jirsa, "Design for shear based on loading conditions", Struct. J., vol. 103, no. 4, pp. 541–550, 2006.

[2] M. P. Collins, E. C. Bentz, and E. G. Sherwood, "Where is shear reinforcement required? Review of research results and design procedures", Struct. J., vol. 105, no. 5, pp. 590–600, 2008.

[3] K.-H. Reineck, E. C. Bentz, B. Fitik, D. A. Kuchma, and O. Bayrak, “ACI-DAfStb Database of shear tests on slender reinforced concrete beams without stirrups”, Struct. J., vol. 110, no. 5, pp. 867–876, 2013.

[4] K.-H. Reineck, E. Bentz, B. Fitik, D. A. Kuchma, and O. Bayrak, “ACI-DAfStb Databases for shear tests on slender reinforced concrete beams with stirrups”, Struct. J., vol. 111, no. 5, pp. 1147–1156, 2014.

[5] M. S. Islam, H. J. Pam, and A. K. H. Kwan, “Shear capacity of high-strength concrete beams with their point of inflection within the shear span”, Proc. Inst. Civ. Eng. Struct. Build., vol. 128, no. 1, pp. 91–99, 1998.

[6] M. P. Collins and D. Kuchma, “How safe are our large, lightly reinforced concrete beams, slabs, and footings?”, Struct. J., vol. 96, no. 4, pp. 482–490, 1999.

[7] N. D. Tung and N. V. Tue, “Effect of support condition and load arrangement on the shear response of reinforced concrete beams without transverse reinforcement”, Eng. Struct., vol. 111, pp. 370–382, 2016.

[8] F. Cavagnis, M. Fernández Ruiz, and A. Muttoni, “An analysis of the shear-transfer actions in reinforced concrete members without transverse reinforcement based on refined experimental measurements”, Struct. Concr., vol. 19, no. 1, pp. 49–64, Feb. 2018.

[9] V. Adam, M. Classen, M. Hillebrand, and J. Hegger, “Shear in continuour slab segments without shear reinforcement under distributed loads”, in fib Symposium. Concrete - Innovations in Materials, Design and Structures, 2019, pp. 1771–1778.

[10] A. P. Caldentey, P. Padilla, A. Muttoni, and Mi. Fernández Ruiz, “Effect of load distribution and variable depth on shear resistance of slender beams without stirrups”, Struct. J., vol. 109, no. 5, pp. 595–603, 2012.

[11] F. J. Vecchio and M. P. Collins, “The Modified Compression-Field Theory for reinforced concrete elements subjected to shear”, J. Proc., vol. 83, no. 2, pp. 219–231, 1986.

[12] M. P. Collins, D. Mitchell, P. Adebar, and F. J. Vecchio, “A general shear design method”, ACI Struct. Journal, vol. 93, no. 1, pp. 36–45, 1996.

[13] A. Muttoni and M. Fernández Ruiz, “Shear strength of members without transverse reinforcement as function of critical shear crack width”, ACI Struct. J., vol. 105, no. 2, pp. 163–172, 2008.

[14] N. D. Tung and N. V. Tue, “A new approach to shear design of slender reinforced concrete members without transverse reinforcement”, Eng. Struct., vol. 107, pp. 180–194, 2016.

[15] Fédération International du Béton (fib), “Model Code 2010”, Ernst & Sohn, 2012.

[16] CSA Committee A23.3, “Design of concrete structures”, Canadian Standards Association, 2014.

[17] E. Bentz, F. J. Vecchio, and M. P. Collins, “Simplified Modified Compression Field Theory of calculating shear strength of reinforced concrete elements”, ACI Struct. J., vol. 103, no. 4, pp. 614–624, Jan. 2006.

[18] SIA, “Code 262 for concrete structures”, Swiss Society of Engineers and Architects, Zürich, Switzerland, 2013.

[19] ACI Committee 318, “Building code requirements for structural concrete (ACI 318-19); and commentary (ACI 318R-19)”, American Concrete Institute, Farmington Hills, 2019.

[20] CEN, EN 1992-1-1:2004, “Eurocode 2: Design of concrete structures – Part 1-1: General rules and rules for buildings”, 2004.

[21] A. Monserrat-López, P. Miguel Sosa, J. L. Bonet Senach, and M. Á. Fernández Prada, “Influence of the plastic hinge rotations on shear strength in continuous reinforced concrete beams with shear reinforcement”, Eng. Struct., vol. 207, 2020.

[22] R. Vaz Rodrigues, A. Muttoni, and M. Fernández Ruiz, “Influence of shear on rotation capacity of reinforced concrete members without shear reinforcement”, ACI Struct. J., vol. 107, no. 5, pp. 516–525, 2010.

[23] UNE EN-12390-3:2009, “Ensayos de hormigón endurecido. Parte 3: Determinación de la resistencia a compresión del hormigón endurecido”, 2009.

[24] UNE EN-12390-6:2010, “Ensayos de hormigón endurecido. Parte 6: Resistencia a tracción indirecta de probetas”, 2010.

[25] UNE EN-12390-13:2014, “Ensayos de hormigón endurecido. Parte 13: Determinación del módulo secante de elasticidad en compresión”, 2014.

[26] UNE-EN ISO 6892-1:2017, “Materiales metálicos. Ensayo de tracción. Parte 1: Ensayo a temperatura ambiente”, 2017.

[27] S. Campana, M. Fernández Ruiz, A. Anastasi, and A. Muttoni, “Analysis of shear-transfer actions on one-way RC members based on measured cracking pattern and failure kinematics”, Mag. Concr. Res., pp. 386–404, 2013.

[28] P. Huber, T. Huber, and J. Kollegger, “Investigation of the shear behavior of RC beams on the basis of measured crack kinematics”, Eng. Struct., vol. 113, pp. 41–58, Apr. 2016.

[29] G. N. J. Kani, “The riddle of shear failure and its solution”, J. Proc., vol. 61, no. 4, pp. 441–468, 1964.